CHAPTER V

PERVAPORATIVE MEMBRANE REACTOR

A pervaporative membrane reactor is one of membrane reactor, while a reaction takes place in liquid phase as water is removed through a polymeric membrane in the permeate stream. The most common reaction system studied for the application of a pervaporative membrane reactor is an esterification reaction between an alcohol and acid.

In this work, a batch reactor integrated with pervaporation developed by Liu and coworkers (2001) has been studied. The batch reactor is used to carry out an exothermic and reversible esterification reaction of acetic acid and butanol. A jacket is used to maintain the temperature of the reactor at a desired set point. Figure 5.1 shows the pervaporative membrane reactor with a jacket.

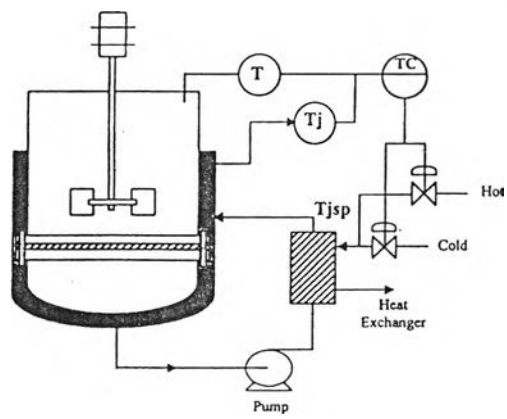

Figure 5.1 A pervaporative membrane reactor

5.1 Mathematical model

The membrane reactor studied by Liu and coworkers (2001) is applied for the esterification of acetic acid and n-butanol to produce butyl actate. This esterification reaction can be presented as follows:

$$A + B \underset{k_2}{\overset{k_1}{\rightleftharpoons}} E + W$$

where A, B, E and W are acetic acid, butanol, butyl acetate and water respectively.

The mathematical model of material and energy balance (Feng and Huang, 1996) is developed to describe the dynamic of pervaporation-based batch reactor and can be shown as follows:

Material Balance for Component i

$$V\frac{dC_i}{dt} + C_i\frac{dV}{dt} = -r_i V - J_i S \qquad (5.1)$$

Where C_i is the concentration of components i within the reactor;

r_i and J_i are the reaction rate and permeation flux through the pervaporative membrane of component i respectively;

V is the reactor volume;

S is the membrane area.

The reaction rate constant of the esterification is obtained from the experimental results by Liu et al., (2001). The reaction rate can be shown as follows:

$$r_i = k_1 C_A C_B C_{cat} - k_2 C_E C_W C_{cat} \qquad (5.2)$$

where C_A,C_B,C_E and C_W are concentration of acetic acid, butanol, butyl acetate and water respectively (mol/l);

C_{cat} is the concentration of catalyst (mol/l);

k_1 and k_2 are rate constant of forward and reverse reactions, respectively.

The rate constant, k_1 and k_2, are described below:

$$k_1 = 4.531 \times 10^6 \exp\left(\frac{-6390}{T_r}\right) \tag{5.3}$$

$$k_2 = 4.376 \times 10^6 \exp\left(\frac{-7090}{T_r}\right) \tag{5.4}$$

The volume change expression of reaction mixtures in the membrane reactor was proposed by Feng and Huang (1996). In addition, when an ideal case is considered that only water can permeate through the membrane during the esterification process, therefore the change of volume can be shown as follows:

$$\frac{dV}{dt} = -\sum_i \frac{J_i M_i}{\rho_i} S \tag{5.5}$$

$$\frac{dV}{dt} = -\frac{J_w M_w}{\rho_w} S \tag{5.6}$$

where M_w and ρ_w are the molar mass and density of water;

J_w is water permeation flux which is assumed to be proportional to water concentration.

The permeation flux through a pervaporation membrane is usually concentration dependent. To simplify the process model, it is assumed that the water flux is proportional to water concentration as seen in the following equation:

$$J_w = P_w C_w \tag{5.7}$$

where P_w is the permeability coefficient of water.

The correlation of temperature-permeability coefficient from experimental data (Liu et al., 2001) is shown below:

$$P_w = exp\left(4.2934 - \frac{1039.24}{T_r}\right) \tag{5.8}$$

By substituting equation (5.6) into equation (5.2), the concentration of the components in the reaction can be determined.

$$-C_i \frac{J_w M_w}{\rho_w} S + V \frac{dC_i}{dt} = -rV$$

$$\frac{dC_i}{dt} = -r + C_i \frac{J_w M_w}{\rho_w} \frac{S}{V} \tag{5.9}$$

The concentration of water can be determined through the following equation:

$$-C_w \frac{J_w M_w}{\rho_w} S + V \frac{dC_w}{dt} = -rV - J_w S$$

$$\frac{dC_w}{dt} = -r - \frac{S}{V} J_w + C_w \frac{J_w M_w}{\rho_w} \frac{S}{V} \tag{5.10}$$

Energy Balance

For temperature control of a batch reactor, a process model relating the reactor temperature, Tr, to the manipulated variable, the jacket temperature, Tj, is required. The energy balance around the reactor contents is given by the following equation:

Reactor :

$$Qr = (-\Delta H)rV \tag{5.11}$$

$$\frac{dT_r}{dt} = \frac{Q_r + UA(T_j - T_r)}{M_r C_{pr}}$$

$$\frac{dT_r}{dt} = \frac{(-\Delta H)rV + UA(T_j - T_r)}{M_r C_{pr}} \tag{5.12}$$

$$M_r = (C_A + C_B + C_E + C_W) \cdot V \tag{5.13}$$

$$C_{pr} = \frac{C_{pA}.C_A + C_{pB}.C_B + C_{pE}.C_E + C_{pW}.C_w}{C_A + C_B + C_E + C_C} \tag{5.14}$$

Jacket:

$$\frac{dT_j}{dt} = \frac{F_j \rho_j C_{pj}(T_j^{sp} - T_j) - UA(T_j - T_r)}{V_j \rho_j C_{pj}} \tag{5.15}$$

where U is the heat transfer coefficient;

A is the heat transfer area;

ΔH is t he heat of reaction;

M_r is the mole of the reactor contents;

C_{pr} is the molar heat capacity of the reactor contents;

F_j is the coolant flow rate;

T_r and T_j are the temperature of reactor and jacket respectively.

It is reasonable that the dynamics of jacket temperature control are approximately first order (Liptak, 1986) with time constant τj and, hence, the *Tjsp (k)*, can be calculated by the following equation:

$$T_{jsp}(k) = T_j(k-1) + \frac{\tau_j}{\Delta t}(T_j(k) - T_j(k-1)) \tag{5.16}$$

where $\tau_j = \frac{q_j}{V_j}$

q_j is the jacket flowrate,

ρ_j is the jacket density,

V_j is the jacket volume,

C_{pj} is the mass heat capacity of the jacket.

Model parameters and an initial operating condition used in the model and control are given in Table 5.1.

Table 5.1 Process parameter values and initial condition

S	= 34 cm^2	C_{PA}	= 124.265 J/mol K	C_{cat}	= 8.9 g/liter
V	= 150 ml	C_{PB}	= 177.025 J/mol K	q_j	= 1 liter/hr
U	= 5 × 104 J/m^2 hr K	C_{PE}	= 2555.5 J/mol K	V_j	= 50 ml
A	= 45 cm^2	C_{PW}	= 75.4 J/mol K	ρ_W	= 1000 g/liter
ΔH	= - 3.97 × 103 J/mol	C_{Pj}	= 4.2 J/g K	ρ_j	= 1000 g/liter
M_w	= 18 g/mol				
		Initial condition			
$C_{A,0}$	= 8.4 mol/l	$C_{E,0}$	= 0 mol/l	$T_{r,0}$	= 298 K
$C_{B,0}$	= 5.47 mol/l	$C_{W,0}$	= 0 mol/l	$T_{j,0}$	= 298 K

5.2 Neural networks in state estimation

Estimation of heat release of reaction

In most Industrial processes, the state variables are not all measurable or, not with sufficient accuracy for control purposes. Furthermore, measurements that are available often contain significant amounts of random noise and systematic errors. For these situations, an estimator has been designed and applied to estimate state variables. Here, the heat releases of reaction (Qr), involved in the determination of the control action, is an unmeasurable variable, so a neural network based estimator has been designed and incorporated with the controller to estimate unmeasurable heat release of reaction. In this work, a multi-layered feed forward neural network has been used as an on-line estimator to estimate the amount of heat release of chemical reactions of the batch reactor. It has been proven to be an accurate and fast on-line dynamic estimator (Aziz et al., 2000). In this case, A multilayered feedforward network is trained by using the Levenberg-Marquardt technique; the feedforward neural network is fed with past historical data, thus the input layers consists of the present and past value of $Tj_{(t)}$, $Tj_{(t-1)}$, $Tr_{(t)}$, $Tr_{(t-1)}$ and $Qr_{(t-1)}$, and the output layer estimates the present value of heat release. The five inputs are fed through the neural network forward model for training and learning. It obtains the output, Qr . 800 input data are used to train the neural network, these are the train set; and 200 input data are used as the test set. The training iteration was set to 1000. The activation function in hidden and output layer are hyperbolic tangent and linear function respectively. The error between output and desired target is used as the training signal for neural network. The estimated Qr is then used in the Neural Network based Controller to estimate the value of $U(t)$.

The selected structure of multilayer feedforward network that has the minimum SSE (sum square error). Table 5.2 presents the SSE for neural network based estimator in each case; one hidden layer with 3, 5, 7, 9, 11 nodes, and two hidden layers with 3, 5, 7, 9, 11 nodes. This selected structure is composed of 5 input-nodes with 2 hidden layers, 7 and 5 nodes (Figure 5.2).

Table 5.2 SSE of neural network based estimator for heat release of reaction

Neurons in 1st hidden layer	**Neurons in 2nd hidden layer**	**SSE** ($x10^{-6}$) (train set)	**SSE** ($x10^{-3}$) (test set)
3	0	0.87918	3.36369
	3	2.8054	3.64506
	5	0.19798	3.51929
	7	0.081270	3.76532
	9	0.21787	3.57133
	11	0.10486	3.06709
5	0	0.077370	3.91338
	3	0.036188	3.78669
	5	0.025468	3.81442
	7	0.19124	3.68467
	9	0.036987	3.88118
	11	0.058283	2.86973
7	0	0.049320	3.58749
	3	0.058697	3.56366
	5	0.062655	2.54139
	7	0.040011	3.54088

Neurons in 1st hidden layer	Neurons in 2nd hidden layer	SSE ($x10^{-6}$) (train set)	SSE ($x10^{-3}$) (test set)
	9	0.019495	3.8391
	11	0.038159	4.03308
9	0	0.11256	2.97813
	3	0.018721	4.38206
	5	0.062077	3.63461
	7	0.036271	3.64492
	9	0.013141	4.53948
	11	0.046293	3.24221
11	0	0.031542	3.89897
	3	0.018475	4.04435
	5	0.031984	4.00384
	7	0.028705	4.85143
	9	0.020285	3.89123
	11	0.040978	3.21351

5.3 Neural network based control

Neural networks are often used in many control configurations; inverse models based control is a one of neural network control configurations. It can be applied in various chemical process plants, because it offers a promising improvement of process modeling and control of nonlinear system. Inverse model is basically the network structure representing the inverse of the system dynamics at the completion of training. The training in this case is called inverse model; this inverse model is

trained by inputs or command signals i.e. set point, past system outputs and past inputs. Moreover, error signals used to train the network is the difference between signals and system outputs; all inputs are fed in the network to predict the output of a process.

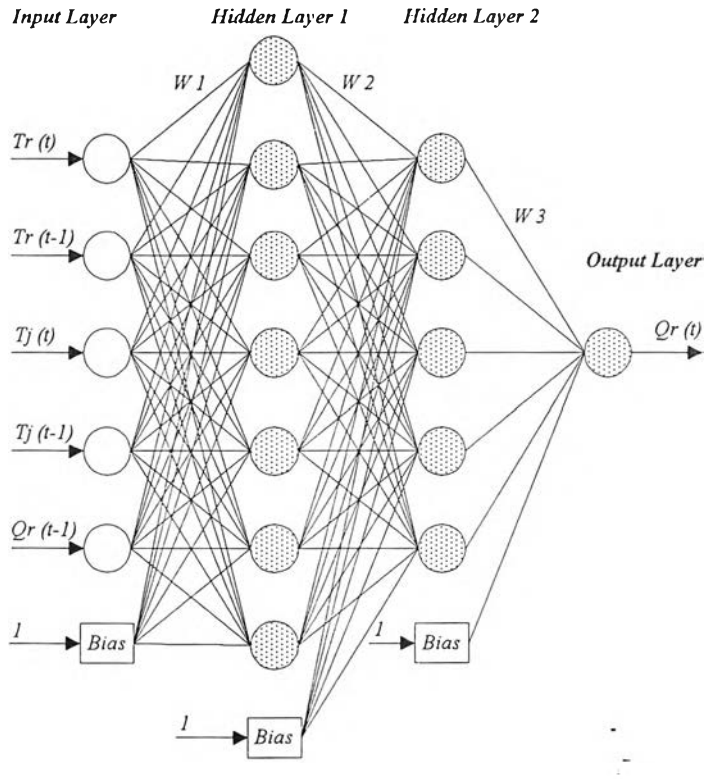

Figure 5.2 Neural network based estimator

For the neural network based inverse model control strategy, the inverse model acts as a controller in cascade under a controlled system or plant. This controller has to learn to supply at its output, appropriate control parameters for a desired target at its input. In this control scheme, the desired set point acts as the desired output which is fed to neural network together with past plant inputs and outputs in order to predict desired current plant inputs (Pao et al., 1992). Neural

network based inverse model control strategy has been investigated in many chemical systems (Hussain et al., 2001).

In this work, a NIMC has been developed to control an optimal temperature (T_r) of a pervaporative membrane reactor for esterification. That the reactor temperature control is very important as it affects the product quality and process operation. 800 input data are used as training set, and 200 input data are used as the test set. The training iteration was set to 1000. The activation function in hidden and output layer are hyperbolic tangent and linear function respectively.

Table 5.3 shows the SSE for neural network inverse model. In this case, the configuration of network with minimum SSE is selected as neural network based controller. Figure 5.3 presents the NIMC configuration with the inputs, hidden and output layers. The configuration is consisting of 5 input-nodes, 11 1st hidden-nodes, 9 2nd hidden-nodes and 1 output-node network.

Table 5.3 SSE of neural network inverse model

Neurons in 1st hidden layer	**Neurons in 2nd hidden layer**	**SSE** ($x10^{-8}$) (train set)	**SSE** ($x10^{-4}$) (test set)
3	0	1.1806	0.82751
	3	0.20235	0.0085336
	5	1.0085	0.442947
	7	4.0018	0.0020357
	9	0.25948	0.0047379
	11	6.2347	0.946301
5	0	0.11315	0.11783
	3	0.56305	0.0264759

Neurons in 1st hidden layer	**Neurons in 2nd hidden layer**	**SSE** ($x10^{-4}$) (train set)	**SSE** ($x10^{-4}$) (test set)
	5	0.73076	0.89673
	7	0.64173	0.270081
	9	0.073711	0.182112
	11	0.28814	0.51301
7	0	0.44143	0.87655
	3	0.25152	0.3720022
	5	0.49863	3.76349
	7	1.1368	4.6952
	9	0.0046821	0.332644
	11	0.072196	1.30621
9	0	0.29583	0.13169
	3	0.018585	0.263365
	5	0.013273	0.254399
	7	0.59287	3.57522
	9	0.0041139	0.00541086
	11	0.0017049	0.00587774
11	0	0.60764	0.14471
	3	0.005307	0.1089
	5	0.004265	0.150074
	7	0.0060895	0.581917
	9	0.0034168	0.00100569
	11	0.11929	0.615228

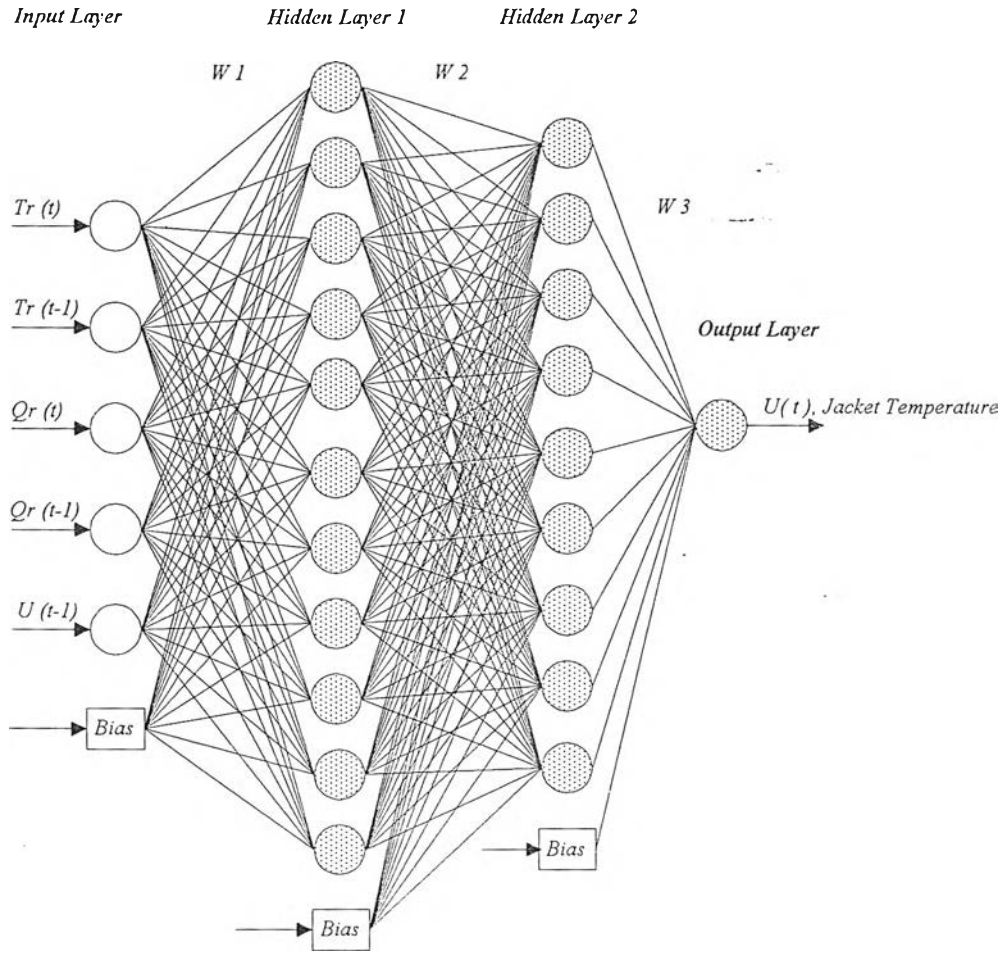

Figure 5.3 Neural network based controller for esterification

Figure 5.4 shows the structure of neural network based inverse model control integrated with neural network based estimator, that utilized in this work.

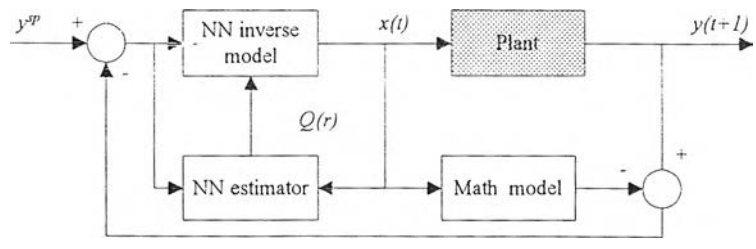

Figure 5.4 Neural network inverse-model-based control strategy

5.4 Control and estimation implementation result

This section demonstrates the simulation studies which are carried out to investigate the performance of NIMC together with a neural network based heat release estimator. The concentration of product C_E at 5.2016 mol/l at the end of batch time which takes up 8 hours is obtained by using neural networks. The objective is to control the optimal temperature set point of pervaporative membrane reactor at 363 K. That the control manipulated input U, represents the jacket temperature while the controlled output is the reactor temperature. The control results of NIMC are also compared with the performance of GMC with Kalman filter (Orladda, 2002).

Figure 5.5 presents the simulation result of open-loop response for the pervaporative membrane reactor where the parameters and constant values are given in table 5.1. The reactor temperature increase with the time from 298 K to 333 K, which does not reach the optimal temperature, 363 K. Therefore, to operate the reactor efficiently, it is necessary to control the reactor temperature to the optimal operating temperature. Figure 5.6 shows the concentration profile of esterification of butanol.

The performance of controller coupled with estimator are simulated in nominal case, in which all model parameter used to simulate are specified correctly, and plant/model mismatch case, in which some parameters have changed from their nominal values. The robustness test in this work can be divided into 9 cases:

- Increase 30% of rate constant, k_1;
- Decrease 30% of rate constant, k_2;

- Decrease 30% of rate constant, k_1;
- Increase 30% of rate constant, k_2;
- Increase 30% of rate constant both k_1 and k_2;
- Increase 30% of heat of reaction, ΔH
- Increase 30% of heat transfer coefficient, U
- Decrease 30% of heat transfer coefficient, U
- Decrease 30% of k_1, k_2 , and increase 30% of U and ΔH

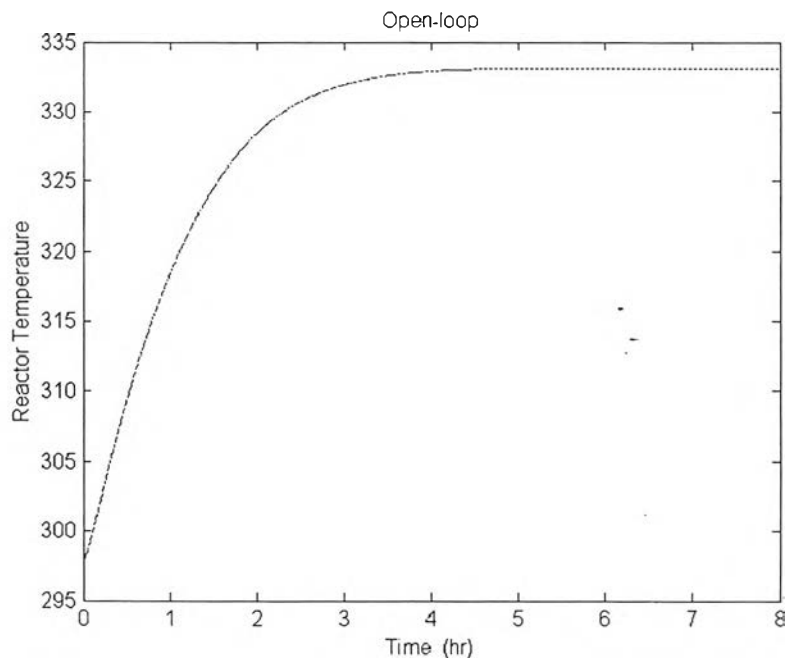

Figure 5.5 Open-loop of pervaperative membrane reactor

In this work, the controller controls the reactor temperature in every 0.01 hours or 36 second, by adjustment the jacket temperature.

1. Control performance is evaluated under nominal condition

Figure 5.7 shows the heat release estimation, and Figure 5.17 shows the response of NIMC in an optimal set point, 363 K. of a pervaporative membrane reactor operating under nominal case. The simulation results have shown that the neural network-based estimator is able to provide good estimate of the unmeasurable heat release. Moreover the NIMC also provides good performance without overshoot in this normal condition. From table 5.4, IAE of the NIMC is slightly better than GMC.couploed with Kalman Filter, so the performance of NIMC and GMC coupled with Kalman Filter is the same. Figure 5.18 shows the control response of GMC with Kalman Filter in nominal case.

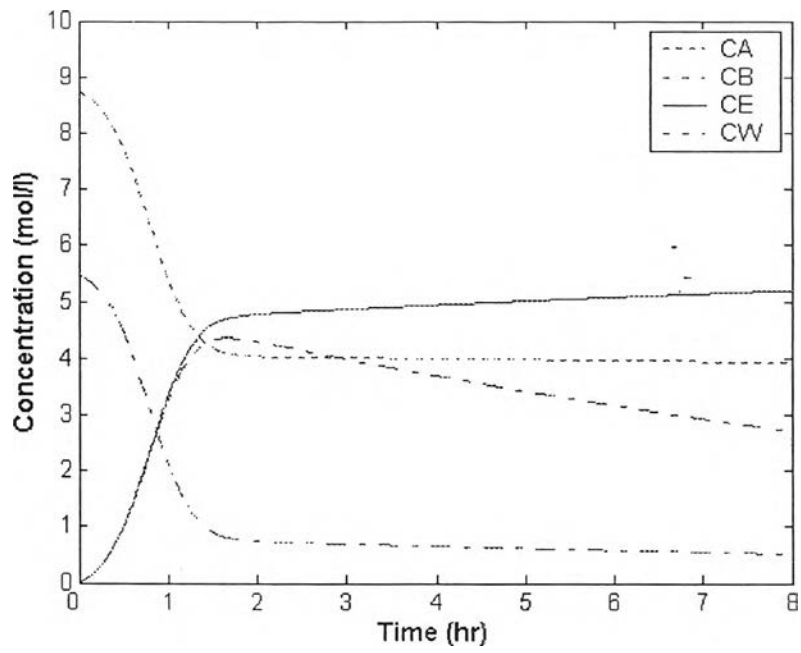

Figure 5.6 Concentration profile

2. Robustness of controller is evaluated by plant mismatch condition

- **Mismatch in rate constant**

When the rate constant, k_1 / k_2 are changed, the results of estimation the heat release is not sensitive (it is still similar nominal condition) because of large value of rate constant both k_1 and k_2. The system can shift to equilibrium faster in case of increase k_1 and decrease k_2.

In this mismatch cases, the NIMC has still provides good control performance. The results of estimation and control by utilizing neural networks are given in Figure 5.8-5.12. Furthermore, the comparison of IAE value between NIMC and GMC coupled with Kalman Filter in Table 5.4 shows that the performance of NIMC as same as GMC coupled with Kalman Filter ; the control responses of NIMC and GMC coupled with Kalman filter are shown in Figure 5.19-5.26. The IAE value in this mismatch is small different from nominal case.

- **Mismatch in heat of reaction**

The result of heat released estimation is shown in Figure 5.13. In this case, heat of reaction has been increased by 30%, the neural network based estimator still provides good estimation result. Heat release by chemical reaction increase with heat of reaction. The NIMC is still robust. However the IAE value of GMC coupled with Kalman filter is slightly better than NIMC. Figure 5.27 and 5.28 show the control responses by using NIMC and GMC coupled with Kalman Filter respectively.

- **Mismatch in heat transfer coefficient**

Figure 5.14 and 5.15 give the simulation results of heat released estimation. Heat released by esterification reaction is sensitive to changing heat transfer coefficient. Heat released by esterification reaction increase when heat transfer coefficient is increased. On the other hand, heat release decrease when heat transfer coefficient is decreased. In case of increasing heat transfer coefficient, the NIMC is found that it provides slightly overshoot response. The IAE value of NIMC is also higher than GMC coupled with Kalman Filter. This is due to uncovering the range of training the networks in all possible process condition. Figure 5.29 – 5.32 show the control responses of NIMC and GMC with Kalman Filter in this mismatch cases.

Table 5.4 The IAE and ISE comparison of Neural network based controller, GMC with Kalman filter

Condition	IAE			ISE		
	NN controller	**GMC**	**% Diff**	**NN controller** ($x10^3$)	**GMC**	**% Diff**
Nominal case	43.5097	45.089	3.5	1.8310	1.864	1.77
+30% k_1	43.4965	44.639	2.5	1.7889	1.839	2.7
-30% k_1	43.5173	-	-	1.8311	-	-
-30% k_2	43.508	45.032	3.4	1.8308	1.863	1.73
+30% k_2	43.509	-	-	1.8310	-	-
+30% k_1 +30% k_2	43.5098	44.702	2.7	1.8310	1.838	0.38
+30% ΔH	44.3305	43.452	1.9	1.8512	1.831	1.09
+30% U	45.7760	36.930	19.32	1.8736	1.531	18.29
-30% U	76.0855	60.261	20.79	2.5268	2.468	2.37
-30% k_1, k_2 +30% $\Delta H, U$	45.5130	36.497	19.81	1.8539	1.524	17.79

- **Mismatch in rate constants, heat of reaction and heat transfer coefficient.**

Figure 5.16 shows the performances of the neural network based estimator for case of mismatch in rate constant, heat of reaction and heat transfer coefficient. Neural network based estimator can estimate heat release precisely. Furthermore, the NIMC is able to provide adequate control, but IAE is higher than GMC controller. The reason of higher IAE is as same as case of mismatch in heat transfer coefficient. Figure 5.33 and 5.34 show the control response of NIMC and GMC controller.

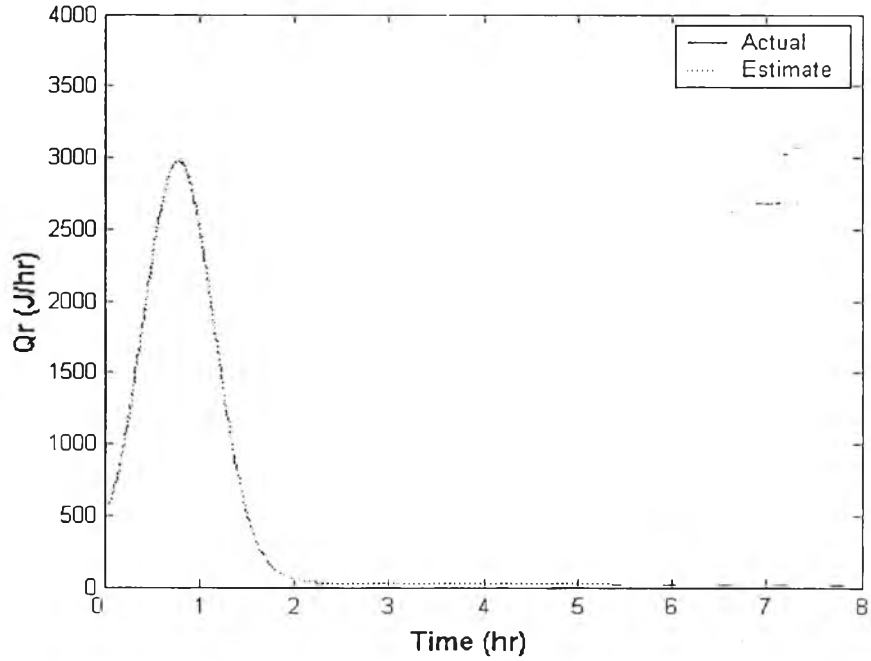

Figure 5.7 Estimates of heat released for nominal case.

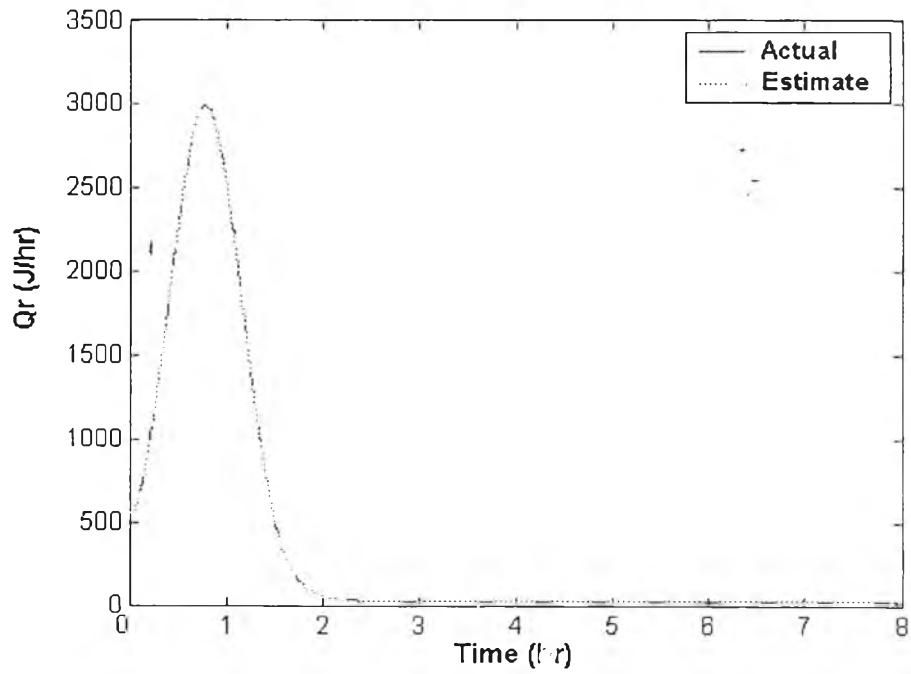

Figure 5.8 Estimates of heat released in plant/model mismatch , +30% *k1*

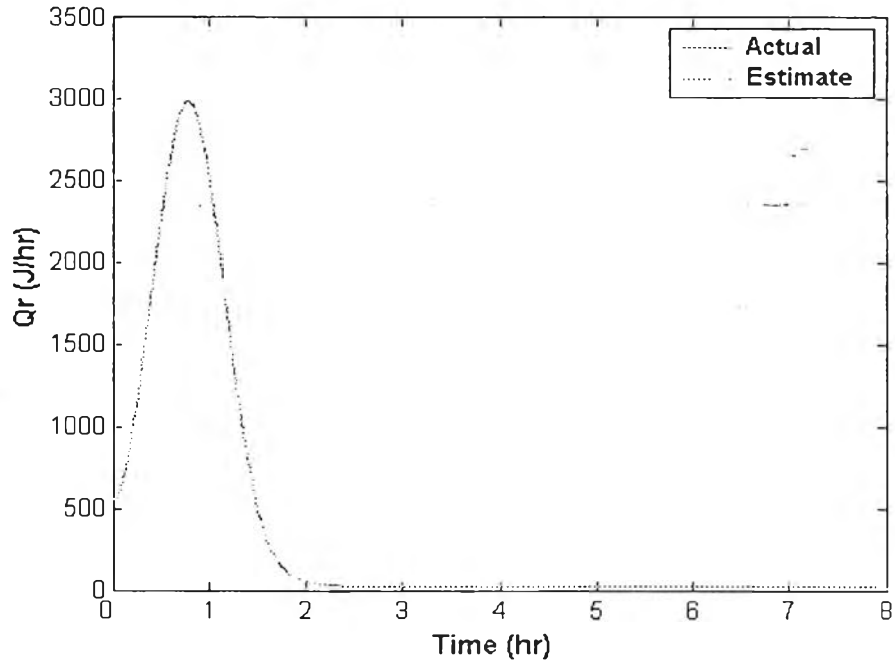

Figure 5.9 Estimates of heat released in plant/model mismatch , -30% *k2* .

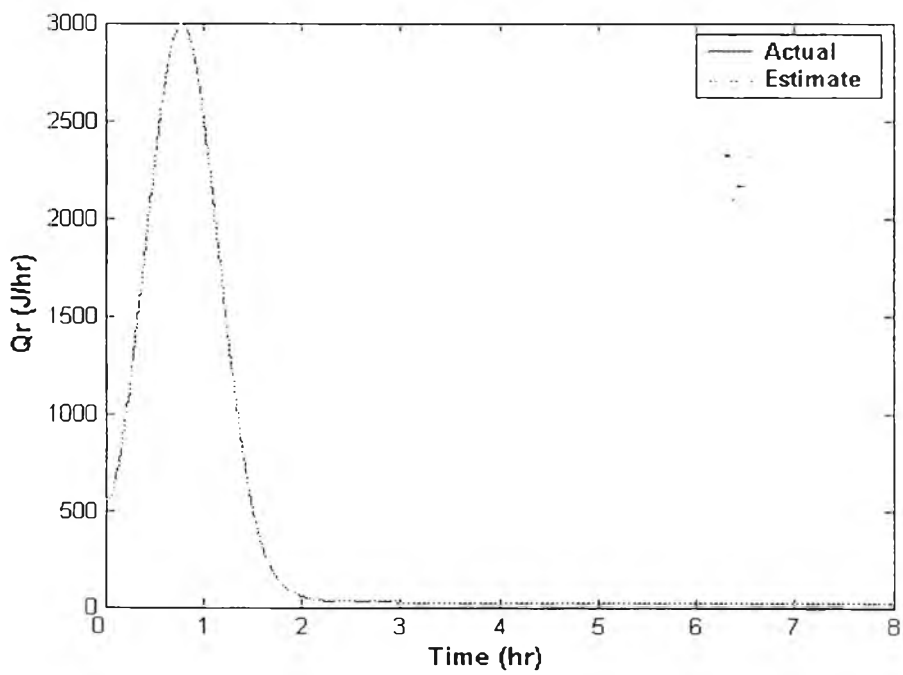

Figure 5.10 Estimates of heat released in plant/model mismatch , -30% *k1*

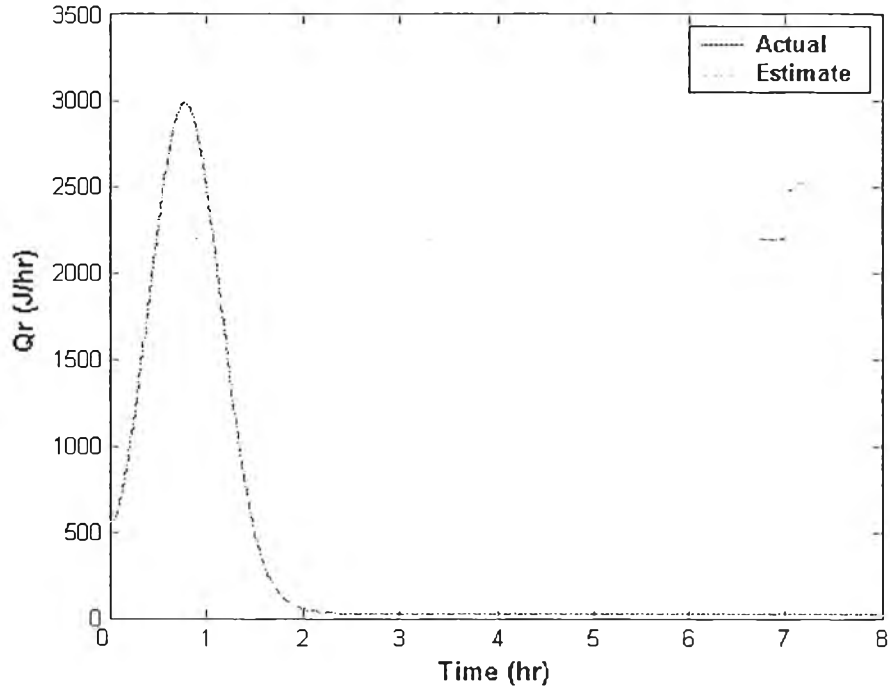

Figure 5.11 Estimates of heat released in plant/model mismatch , +30%*k2*

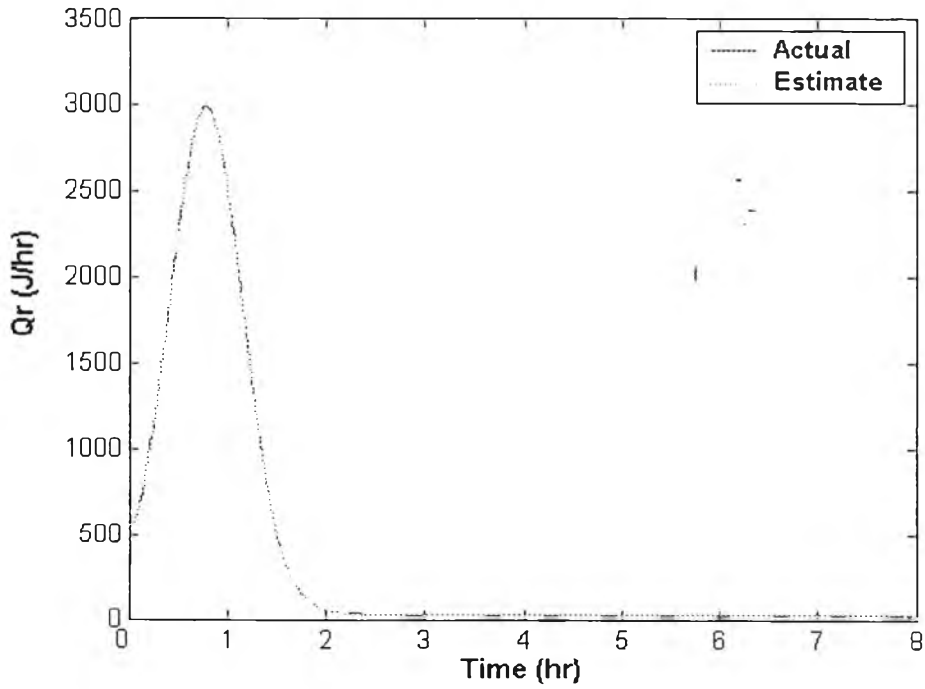

Figure 5.12 Estimates of heat released in plant/model mismatch , +30% k1, +30%*k2*

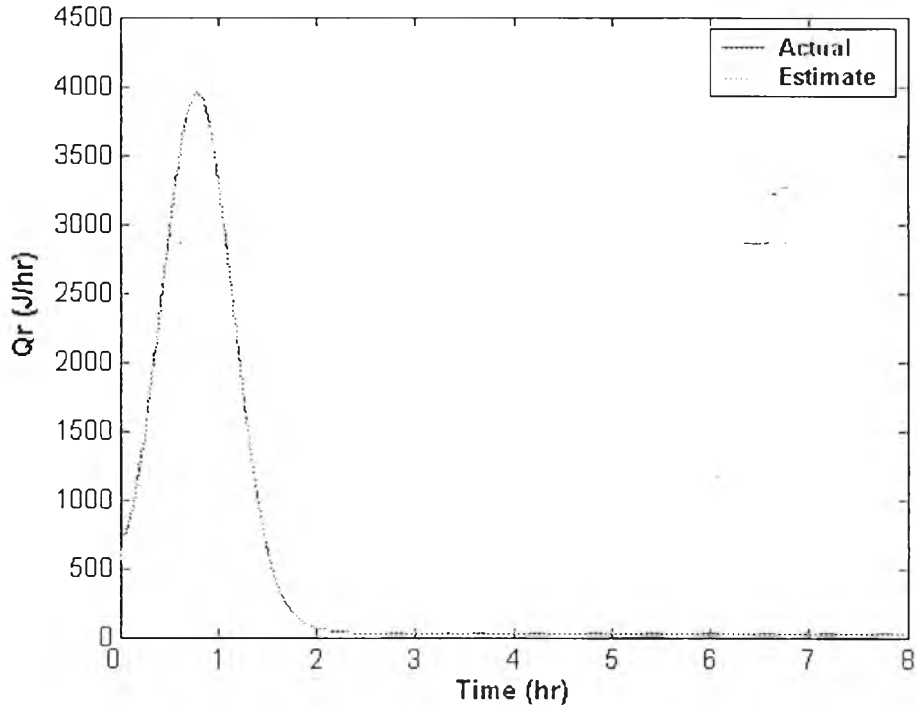

Figure 5.13 Estimates of heat released in plant/model mismatch , +30% ΔH

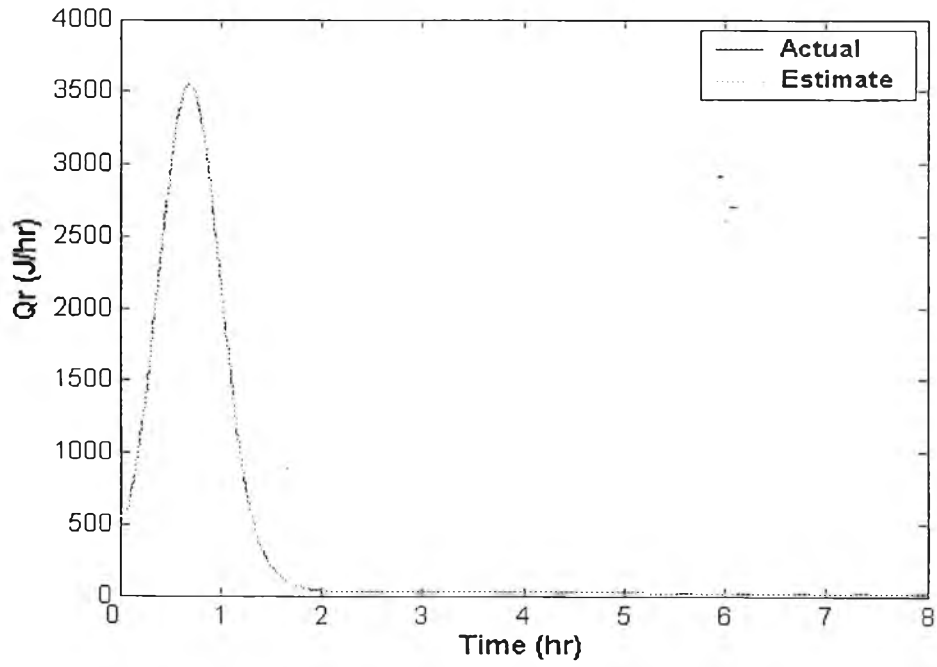

Figure 5.14 Estimates of heat released in plant/model mismatch , +30% U

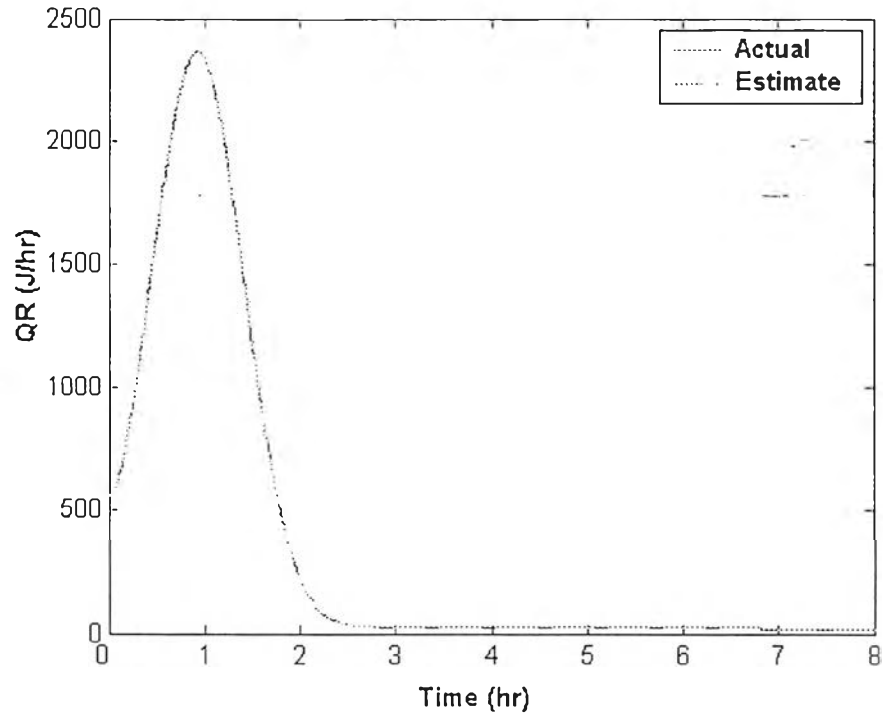

Figure 5.15 Estimates of heat released in plant/model mismatch , -30% *U*

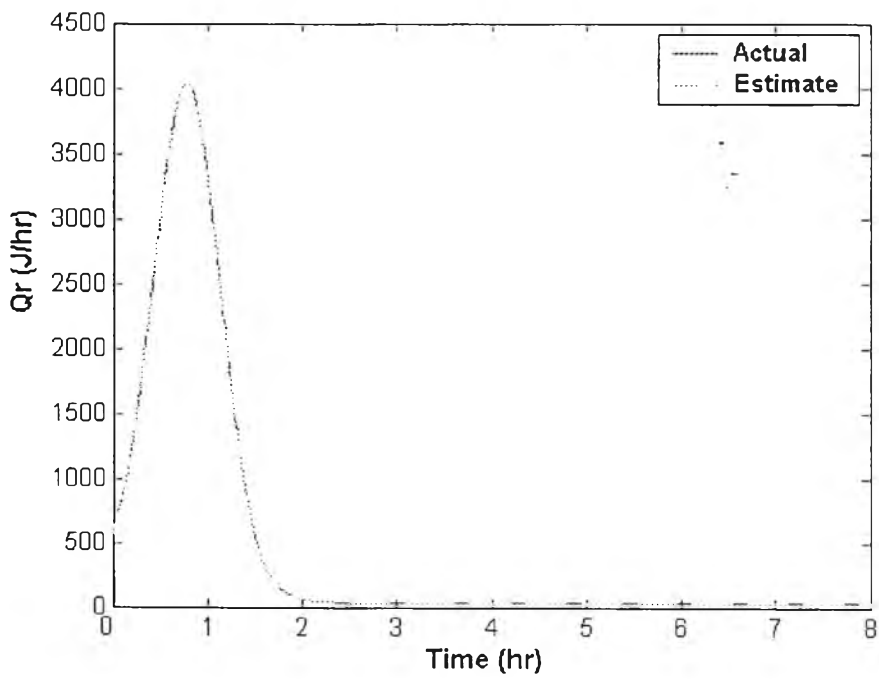

Figure 5.16 Estimates of heat released in plant/model mismatch , *-30% k1,k2 and +30%Δ H, U*

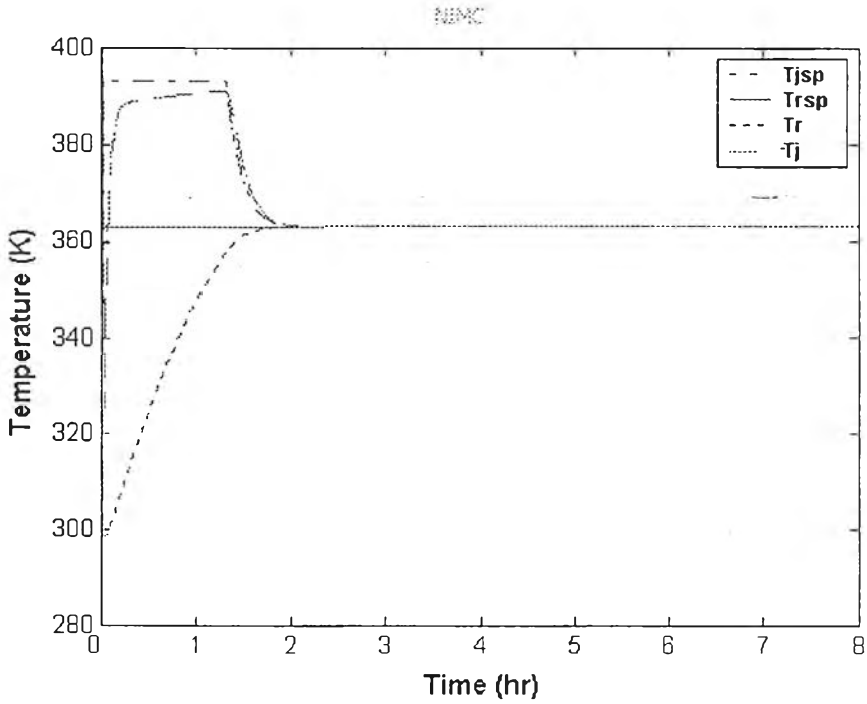

Figure 5.17 Response of pervaporative membrane reactor for nominal case.*(NN)*

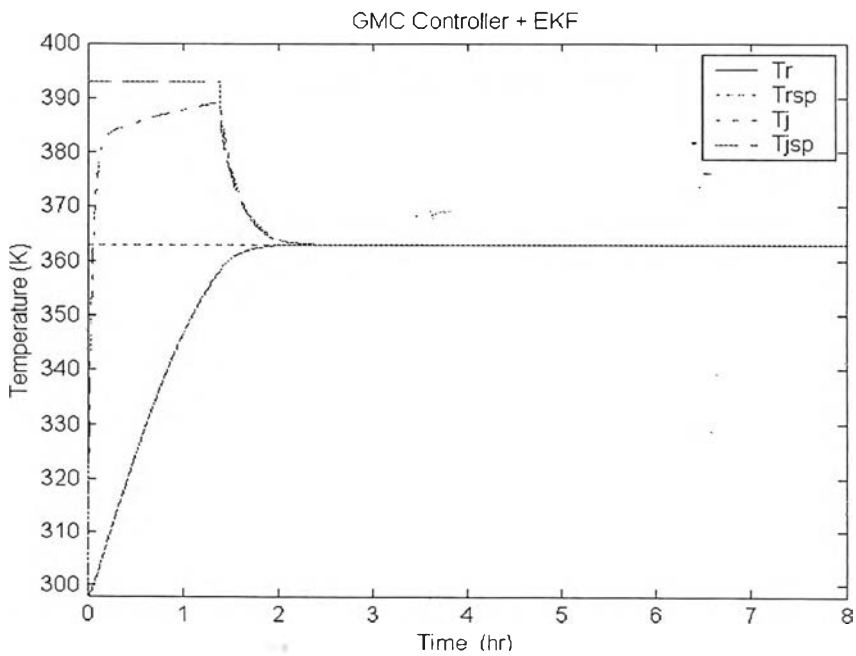

Figure 5.18 Response of pervaporative membrane reactor for nominal case.*(GMC, Orladda, 2002)*

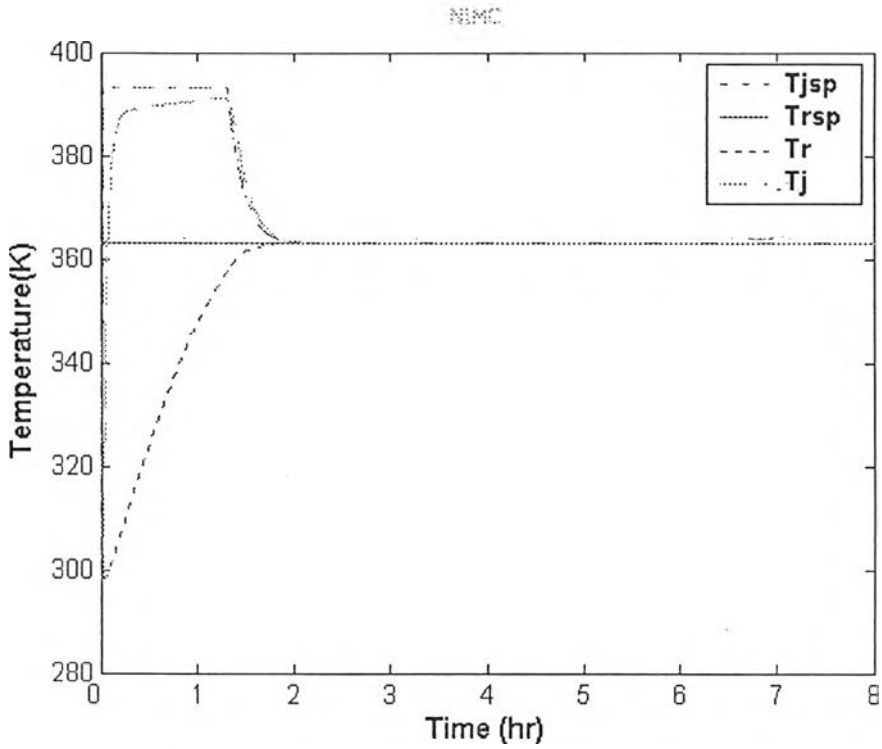

Figure 5.19 Response of pervaporative membrane reactor in plant/model mismatch , +30% *k1 (NN)*

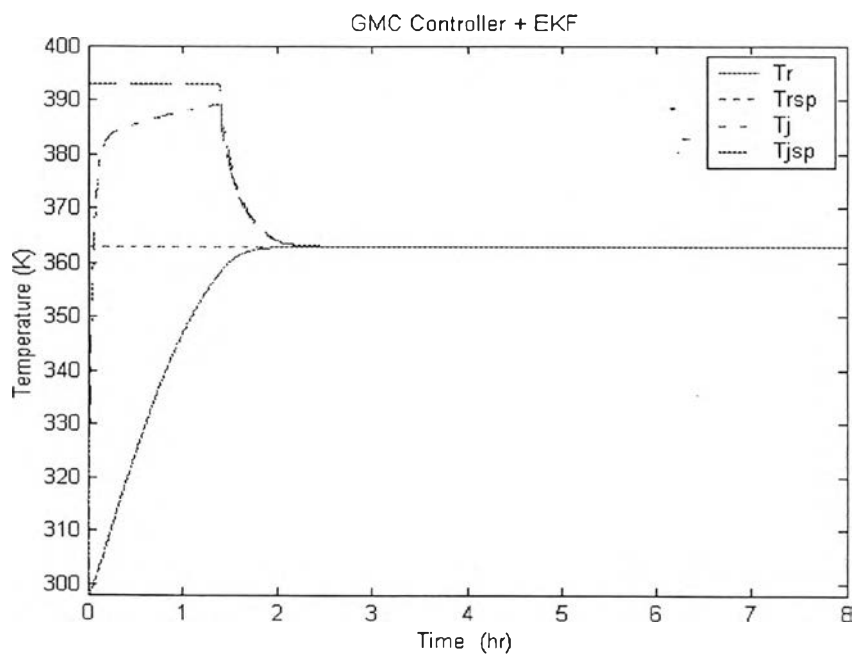

Figure 5.20 Response of pervaporative membrane reactor in plant/model mismatch , +30% *k1 (GMC, Orladda, 2002)*

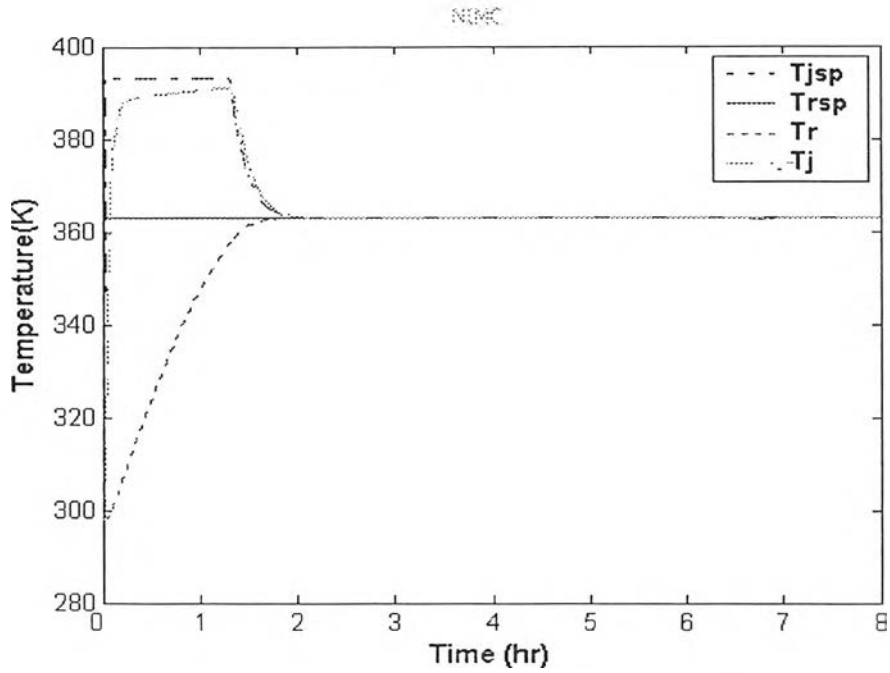

Figure 5.21 Response of pervaporative membrane reactor in plant/model mismatch , -30% *k2 (NN)*

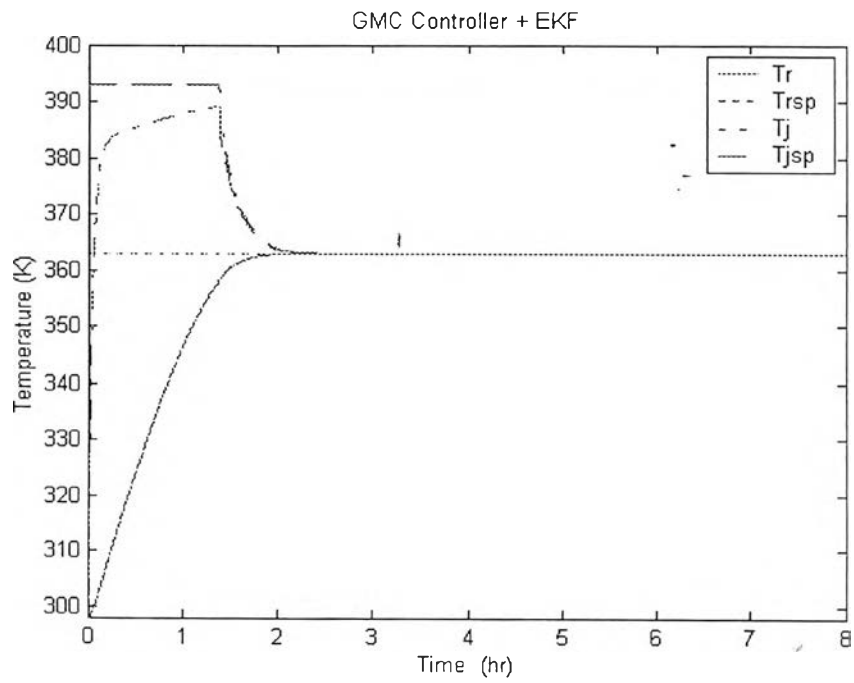

Figure 5.22 Response of pervaporative membrane reactor in plant/model mismatch , -30% *k2 (GMC, Orladda, 2002)*

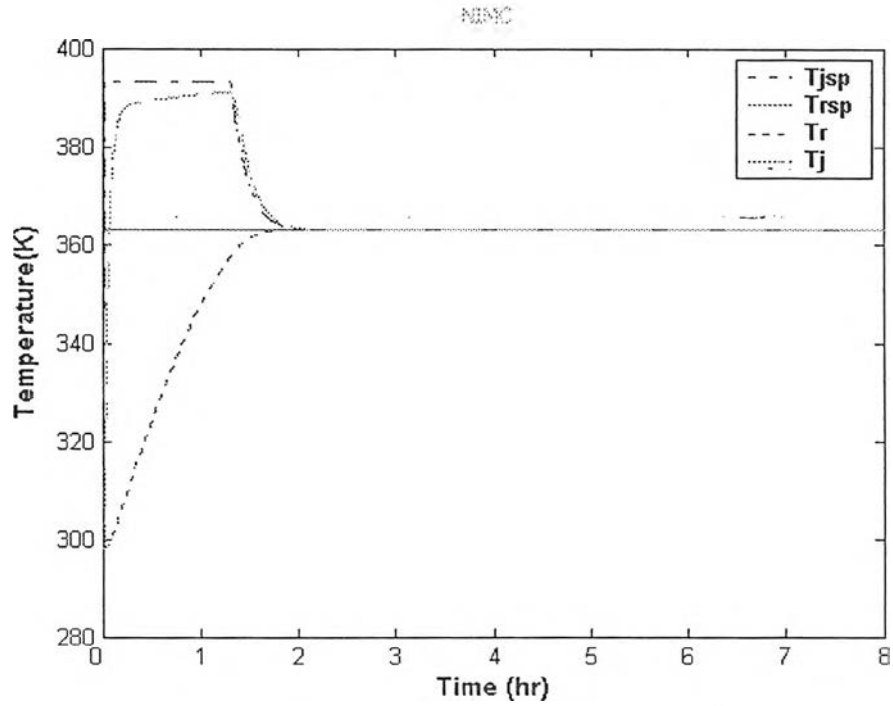

Figure 5.23 Response of pervaporative membrane reactor in plant/model mismatch , -30% *k1 (NN)*

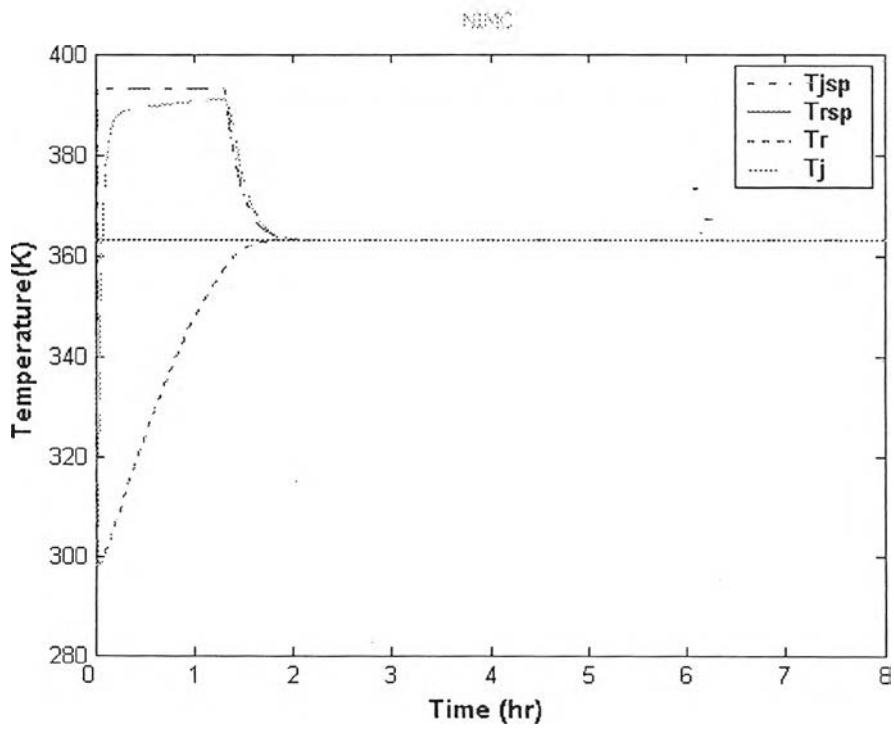

Figure 5.24 Response of pervaporative membrane reactor in plant/model mismatch , +30% *k2 (NN)*

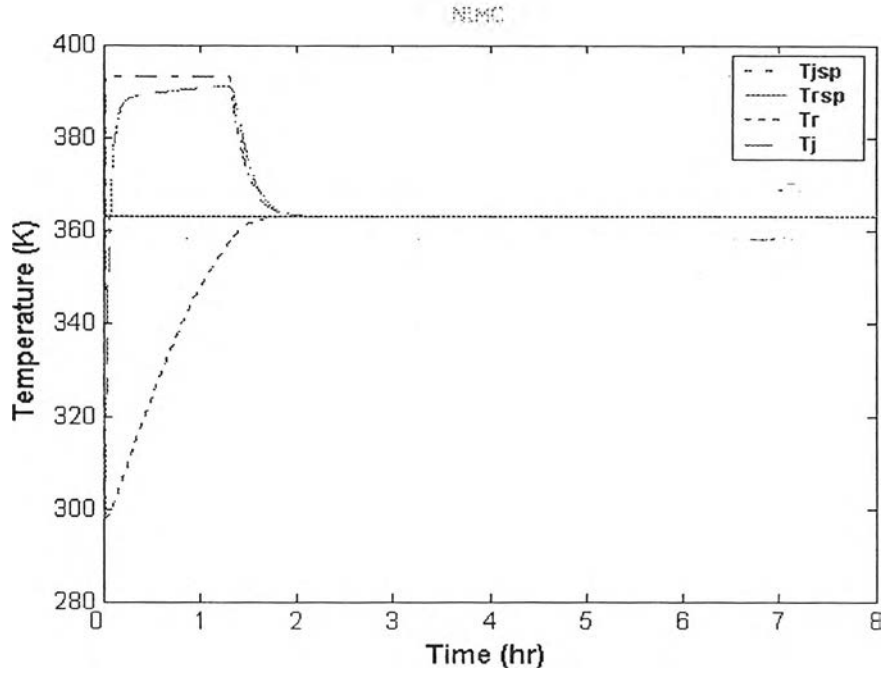

Figure 5.25 Response of pervaporative membrane reactor in plant/model mismatch , +30% k1, +30%*k2 (NN)*

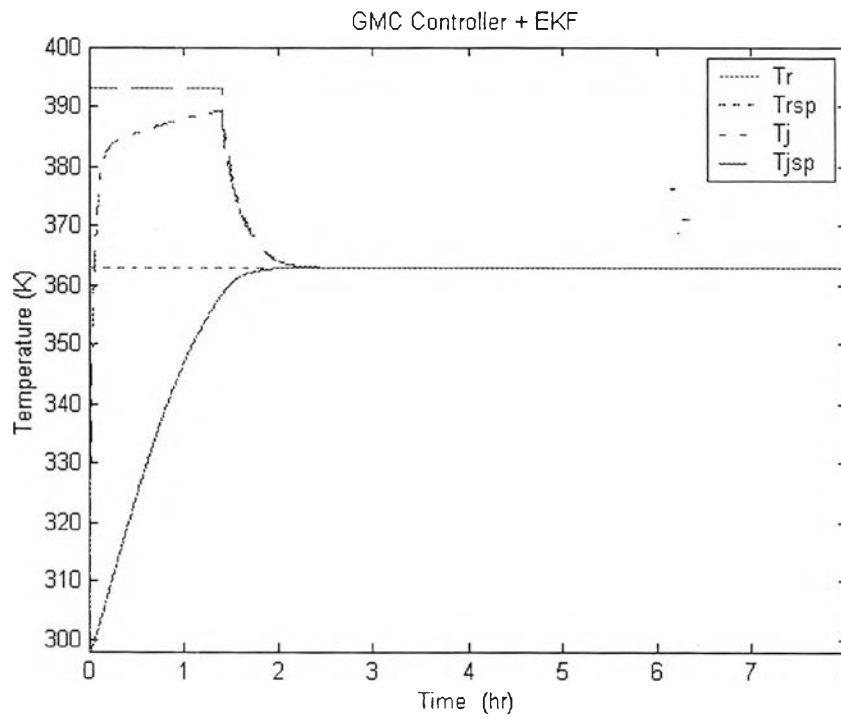

Figure 5.26 Response of pervaporative membrane reactor in plant/model mismatch , +30% k1, +30%*k2 (GMC, Orladda, 2002)*

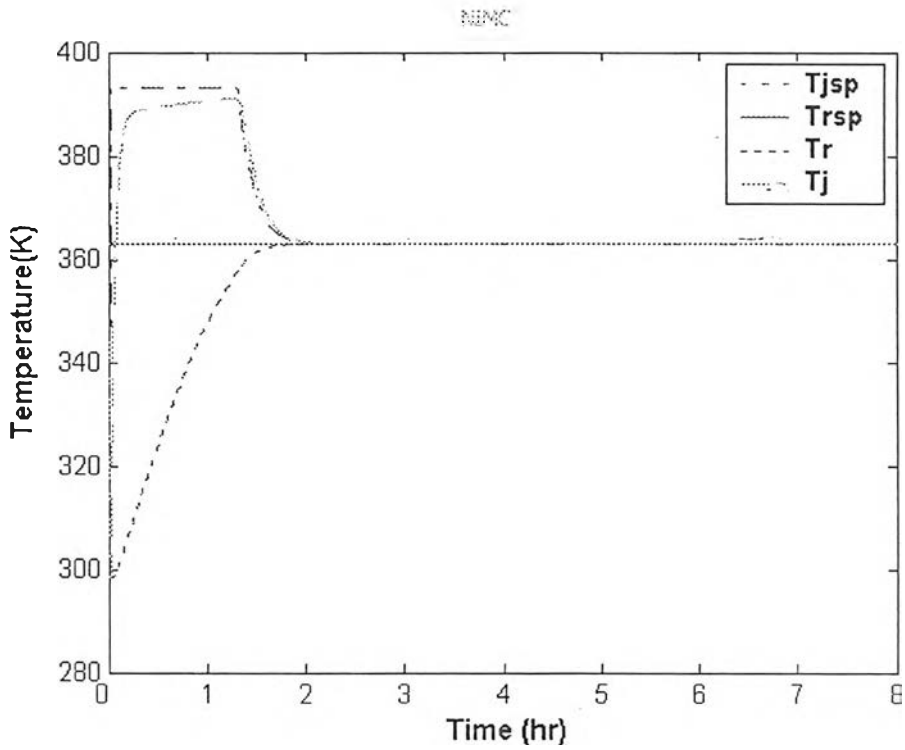

Figure 5.27 Response of pervaporative membrane reactor in plant/model mismatch , +30% *ΔH (NN)*

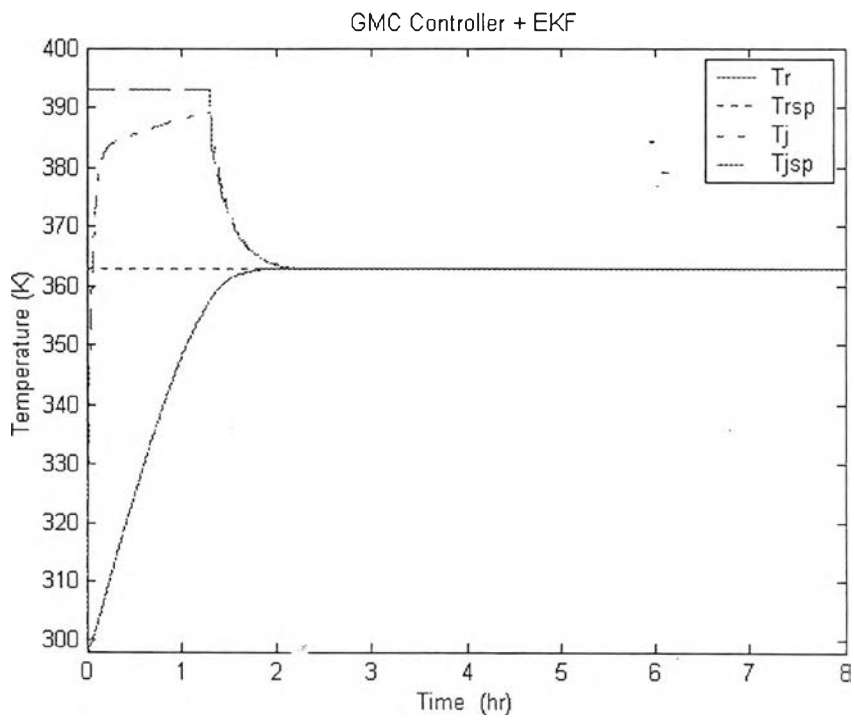

Figure 5.28 Response of pervaporative membrane reactor in plant/model mismatch , +30% *ΔH (GMC, Orladda, 2002)*

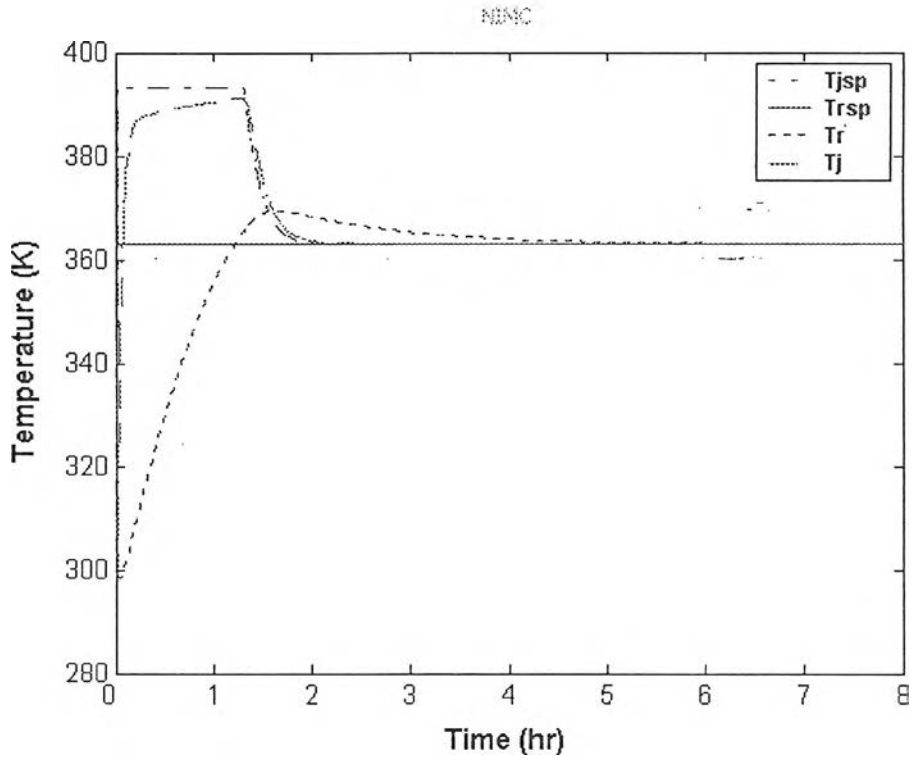

Figure 5.29 Response of pervaporative membrane reactor in plant/model mismatch , +30% *U (NN)*

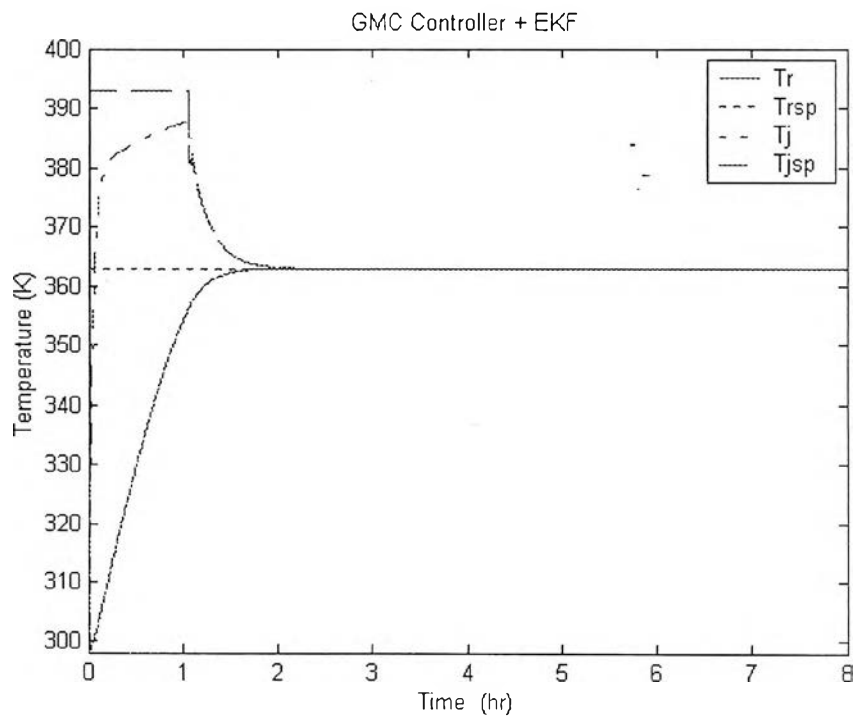

Figure 5.30 Response of pervaporative membrane reactor in plant/model mismatch , +30% *U (GMC, Orladda, 2002)*

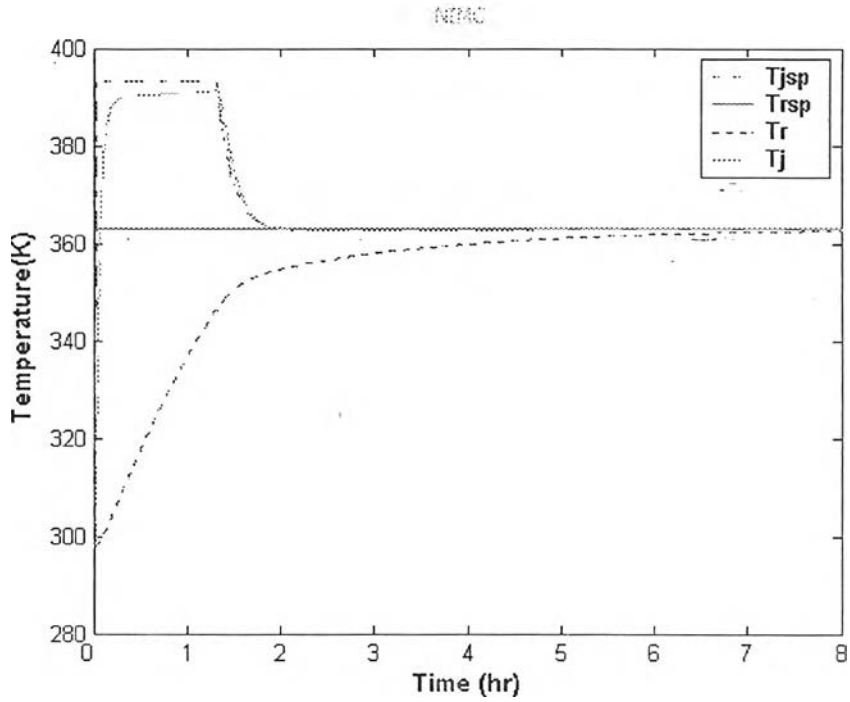

Figure 5.31 Response of pervaporative membrane reactor in plant/model mismatch , *-30% U (NN)*

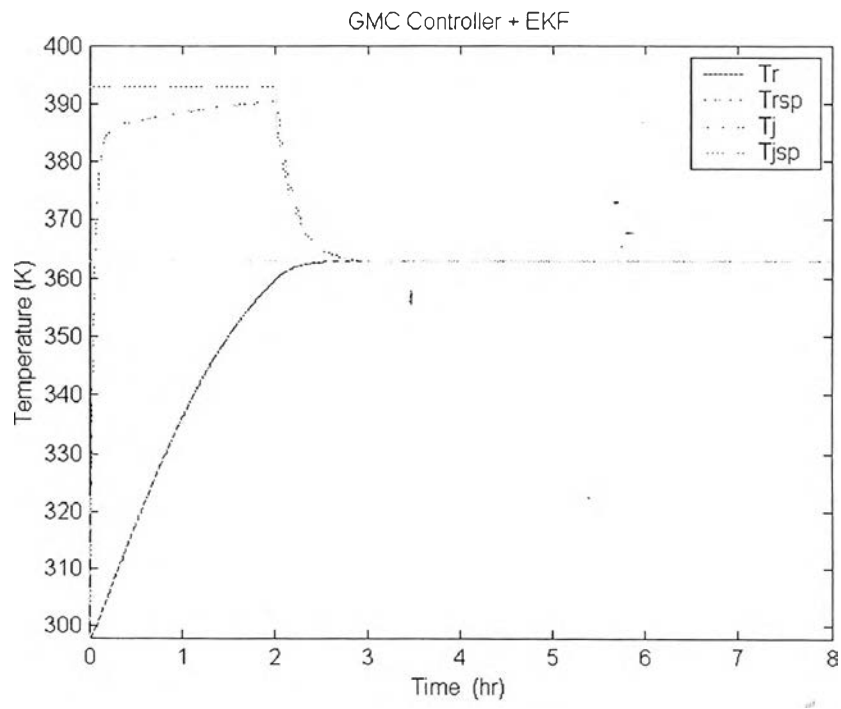

Figure 5.32 Response of pervaporative membrane reactor in plant/model mismatch , *-30% U (GMC, Orladda, 2002)*

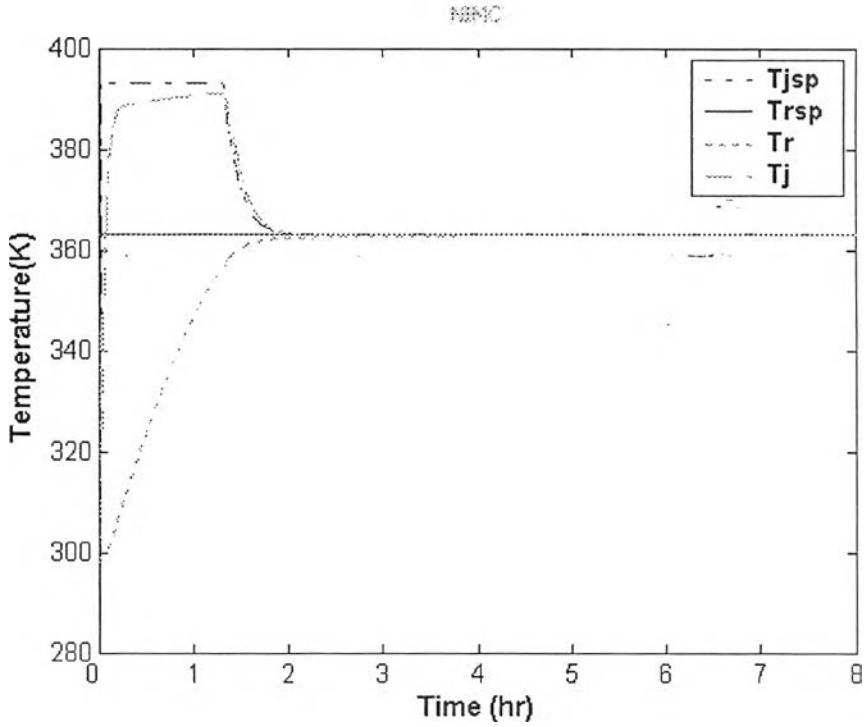

Figure 5.33 Response of pervaporative membrane reactor in plant/model mismatch , *-30% k1,k2 and +30%Δ H, U (NN)*

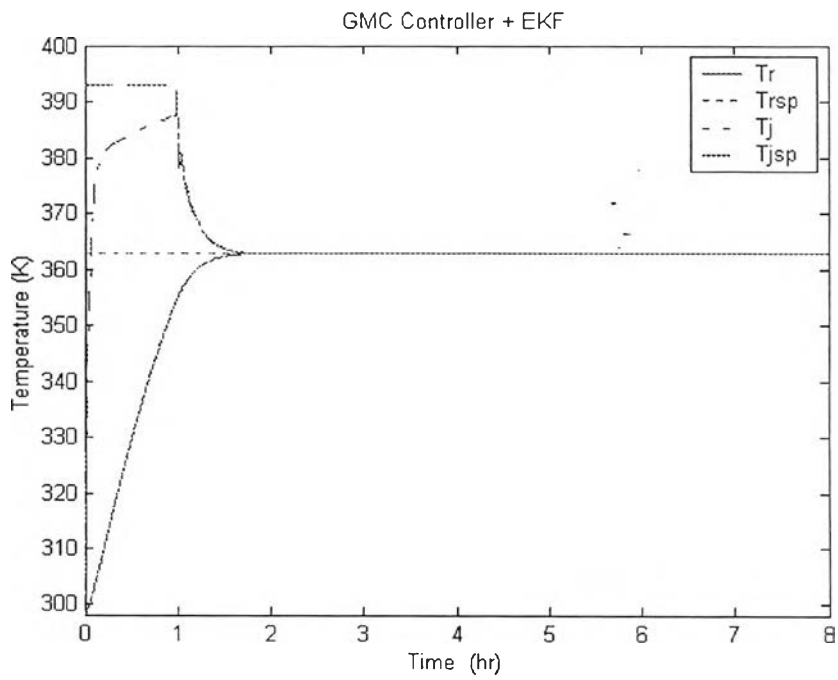

Figure 5.34 Response of pervaporative membrane reactor in plant/model mismatch , *-30% k1,k2 and +30%Δ H, U (GMC, Orladda, 2002)*